Real Time Hypoxia Prediction using Decision Fusion

Sayandeep Acharya*, Arjun Rajasekar*, Barry S. Shender†, Leonid Hrebien* and Moshe Kam‡

* Department of Electrical and Computer Engineering
Drexel University, Philadelphia, Pennsylvania 19104, USA
Email:{sa427@, ar924@, lhrebien@ece.}drexel.edu
†Human Systems Department
Naval Air Warfare Center Aircraft Division, Patuxent River, MD 20670, USA
Email: barry.shender@navy.mil
‡Department of Electrical and Computer Engineering
Newark College of Engineering
New Jersey Institute of Technology, New Jersey 07102, USA
Email: kam@njit.edu

Abstract—Humans who operate in high altitudes for prolonged durations often suffer from hypoxia. The commencement of physiological and cognitive changes due to the onset of hypoxia may not be immediately apparent to the exposed individual. These changes can go unrecognized for minutes and even hours, and may lead to serious performance degradation or complete incapacitation. A dynamic system capable of monitoring and detecting decreased physiologic states due to the onset of hypoxia has the potential to prevent adverse outcomes. In this study we develop a real time hypoxia monitoring system based on a parallel M-ary decision fusion architecture. Blood oxygen saturation levels and altitude readings are the inputs and estimates of the level of hypoxia are the outputs. We develop new temporal evolution models for blood oxygen saturation and functional impairment with respect to varying altitude. The proposed models enable accurate tracking of various hypoxia levels based on the duration of stay of the subject at an altitude. Using a Bayesian decision-making formulation, the system generates global estimates of the degree of hypoxia. The detection system is tested against synthetic and real data sets to demonstrate applicability and accuracy.

Index Terms—Hypoxia, Decision Fusion, Data Fusion, Functional Impairment, Time of Useful Consciousness, Pulse Oximeters.

I. INTRODUCTION

HYPOXIA is diminished availability of oxygen to the cells of the body [1]. It can occur due to inadequate oxygenation of the lungs for extrinsic reasons, deficiency of oxygen in atmosphere, venous-to-arterial shunts (intra pulmonary or intra cardiac), inadequate transport and delivery of oxygen, or inadequate tissue oxygenation or oxygen use. Decreased oxygen availability in brain tissues can cause mild to severe deterioration in cognitive functional abilities, leading to impairment and, eventually, incapacitation. Hypoxia occurs most commonly in people exposed to high altitudes, performing strenuous exercise, or working for prolonged periods of time at high altitudes. Individuals at risk of hypoxia include military ground personnel involved in high altitude mountain operations, helicopter pilots and emergency medical personnel involved in high altitude casualty evacuation activities and high performance aircraft pilots who engage in high G aerial combat maneuvers. Commencement of physiological and cognitive changes may not be apparent to the affected individual, and can go unrecognized, potentially leading to serious performance degradation or even complete incapacitation. A dynamic system capable of detecting degraded physiologic reserve thus has the potential to help prevent or mitigate such adverse outcomes.

The most common and easiest way to determine the presence of hypoxia is by measuring the blood oxygen saturation (SpO_2). A healthy human has on average a SpO_2 value of 95-100%. SpO_2 values below 90% are considered low, and are taken as a possible indication of onset of hypoxia. The most common non-invasive device used to measure blood oxygen saturation levels is the pulse oximeter. This device uses a photo detector to measure the difference in the extinction curves of hemoglobin and oxygenated hemoglobin using reflected or transmitted light of different wavelengths absorbed in peripheral skin tissues [2], [3]. The common types of oximeters are applied either on the finger or on the forehead of the subject being monitored.

Hypoxia monitoring has been reported in several previous studies. A hypoxia detection and warning system was patented as an Aviation Hypoxia Monitor [4], which has a single pulse oximeter attached to the ear. It provides visual and audio signals if the blood oxygen level of a subject decreases significantly. The Hypoxia Detection and Warning System described in [5] is composed of an electrochemical oxygen sensor located within the breathing mask of a pilot. It provides a vibratory warning within the mask when partial pressure of oxygen in the system falls below a set point. In [6], a personal hypoxia monitoring system was presented which uses the cross-correlation between heart rate, respiratory rate, blood flow velocity and blood oxygen saturation levels to identify the onset of hypoxia.

Pulse oximeters are widely used in operating rooms, as

emergency medical aids, and to monitor ambulatory heart and respiratory-system patients. However, these devices are prone to inaccuracies due to several sources, most notably light scattering inside blood tissues. They are also affected by noise artifacts due to motion, ambient light interference, respiratory maneuvers, and pooling of blood at the point of measurement due to body orientation. Furthermore, depending on the manufacturer, pulse oximeters differ in the measurement algorithms they employ and their individual noise characteristics [7], [8] resulting in varied reliabilities. In situations where fast and reliable hypoxia detection is required, a single pulse oximeter may therefore not be sufficient, and it may be advantageous to use a combination of several such devices. A multi detector approach may aid in reducing the impact of random noise and also in leveraging the best features of each individual device. Moreover, instead of just comparing a single saturation level reading to a 90% threshold to predict hypoxia, it is may be useful to have the system predict the degree of severity of hypoxia according to a pre-defined scale, and track time evolution of the prediction.

In a study conducted at the Naval Air Warfare Center Aircraft Division (NAWCAD) [9], three oximeters from different manufacturers were used simultaneously to monitor human volunteers exposed to altitudes ranging from 0 to 18000 ft. These were Respironics Novametrix 515B (transmittance type on finger), and two reflectance type oximeters — Nonin pulse oximeter 9847 and Masimo Rad-87 (used on the forehead).

This paper describes the processing of observations from these three oximeters and develops a multi hypothesis decision fusion framework to integrate their outputs. To design the fusion system, we propose new temporal evolution models for blood oxygen saturation and functional impairment with respect to varying altitude which enable accurate tracking of various hypoxia levels. To the best of our knowledge, such a study has not been carried out in the aerospace medicine community so far. Our proposed blood oxygen saturation model achieved a root mean square (rms) error of 2.45% when fitted against a real data set, compared to a rms error of 5.43% of an existing theoretical model [10] (which predicts evolution of blood oxygen saturation levels as a function of altitude).

In our proposed architecture local detectors associated with each oximeter generate local decisions independently, each detector identifying the most likely category of hypoxia present. A fusion center combines these local decisions to a global decision about the severity of the observed hypoxia. Detection and fusion occur in real time and the system can achieve continuous monitoring of the hypoxic state of an individual. This detection framework was tested with both simulated and real data sets. When prior probabilities of hypotheses were estimated from duration of stay at an altitude, the three local detectors had average error rates of 0.0429, 0.1091 and 0.0692 respectively, whereas the fusion center achieved an error rate of 0.0390. This is a 9% improvement over the best local detector.

In Section II, we review the data collection process and provide a detailed description of the fusion system design and our temporal evolution models for blood oxygen saturation. In Section III, we discuss the results of testing the fusion system using real data and assess its performance. Section IV provides future research directions. A summary of the main contributions and concluding remarks are provided in Section V.

II. METHOD

A. Data Collection

In a study [9] conducted at NAWCAD, informed consent[1] was obtained and 45 datasets from 26 volunteers (4 women and 22 men) were collected. The subjects were exposed to a varying normobaric altitude profile, ranging from 0 to 18,000 ft, simulated using a Reduced Oxygen Breathing Device (ROBD). The experimental profile was the following: ascent at 1000 ft·s^{-1}(304.8 m·s^{-1}) to 10,000 ft (3048 m); hold for 10 min; ascent to 18,000 ft (5486.4 m) at the same rate and hold for 20 min; and descent at the same rate to ground level. The volunteers spent up to 20 min at the equivalent of a maximum altitude of 18,000 ft (5486.4 m), during which time the data from a finger pulse oximeter (Respironics Novametrix 515B, Murrysville, PA) and two forehead pulse oximeters (Nonin 9847, Plymouth, MN, and Masimo RAD-87, Irvine, CA) were recorded. Subjects were exposed to one or two repetitions of the profile. Early exposure termination criteria included subject request, finger SpO_2 below 60% for 10 seconds, or unresponsiveness.
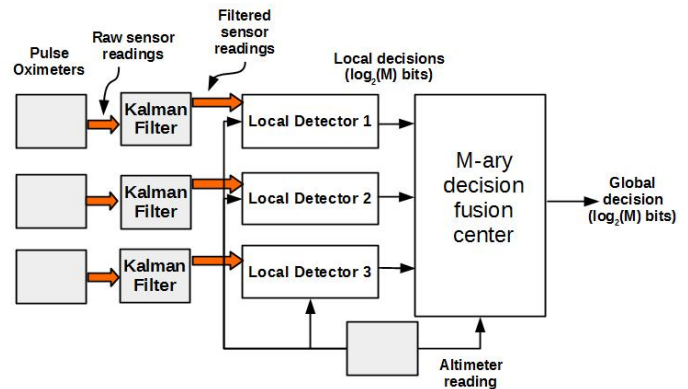
B. Fusion Setup

Figure 1: M-ary decision fusion setup with 3 pulse oximeters.

The M-ary fusion set up is shown in Fig. 1. It consists of three ($N = 3$) pulse oximeters (Finger Pulse, Nonin and, Masimo) arranged in a parallel configuration, each measuring blood oxygen saturation levels. The raw readings are smoothed by state-augmented Kalman filters, one for each oximeter signal. A brief summary of the Kalman filter model is provided in Appendix A, and further details can be found in [11]. Each oximeter also has an associated local detector that receives the filtered oxygen saturation levels. An altimeter provides altitude readings to all the local detectors and the fusion

center. The altimeter readings allow the fusion center and the local detectors to calculate the altitude and the corresponding duration of stay of the subject at that altitude. As will be discussed later in section II-C3, the information derived from the altitude can also help in generating reliable predictions about the likelihood of a hypoxia level.

Using a local decision rule, the local detector decides on the most likely category of hypoxia and sends forward this decision to the fusion center. We use five ($M = 5$) hypoxia levels represented by the set of hypotheses H_1, H_2, H_3, H_4, H_5, in this (increasing) order of severity of hypoxia (refer to Table I). The fusion center uses the local decisions and the altimeter readings to arrive at a global decision accepting one of the hypotheses (one of the M hypoxia categories). For a M hypotheses fusion scheme, all decisions (local and global) can be represented using $\lfloor log_2(M) \rfloor + 1$ bits, where $\lfloor . \rfloor$ is a floor function (floor of a real number v is the largest integer not greater than v).

1) Severity of Hypoxia Gradations: At high altitudes, without adequate oxygen supply as available at sea level, an individual may lose the ability to perform physical tasks efficiently and suffer from impaired judgment. This loss of ability is termed functional impairment, and is expressed in percentage and denoted here by $\%FI \in[0 \ 100]$. We have used the gradations presented in [12], (page 39, Fig. 2-3) to group various percentage functional impairment ranges with the most probable corresponding symptoms. Table I shows the ranges of SpO_2 and $\%FI$ based on which the hypoxia severity gradations were defined for this study. The third column shows the probable symptoms corresponding to the various ranges of functional impairment.

Next we outline the detection and fusion algorithms at the local detectors and the fusion center. For more details see [13]. The local detectors use decision rules to independently minimize the M hypotheses Bayes' risk defined as

$$\mathcal{R} = \sum_{i=1}^{M} \sum_{j=1}^{M} P_j C_{ij} \int_{Z_i} p(x|H_j)dx, \qquad (1)$$

where P_j, $j = 1, ..., M$ are the prior probabilities of the hypotheses, C_{ij} is the cost of choosing hypothesis H_i when hypothesis H_j is true. The observations are denoted by x; Z_i is the region in the observation space where the decision rule assigns all points to hypothesis H_i; and $p(x|H_j)$ is the probability density of the observation conditioned on the hypothesis H_j. The local detector error rates are assumed to be fixed and can be calculated once the decision rules are determined. The fusion center uses the local decisions as inputs and computes a global decision such that the global average cost or Bayes' risk ($\mathcal{R}$) in (1) is minimized. In this study, we assume the following symmetrical cost assignments:

$$C_{ij} = \begin{cases} 0, & i = j \\ 1, & i \neq j. \end{cases} \qquad (2)$$

Under this cost assumption, $\mathcal{R}$ is the average probability of error.

2) Local Decision Rule: We denote the observations at the jth local detector by x_j. To make a local decision at detector j, the following test statistic is computed $\forall i = 1, ..., M; j = 1, ..., N$:

$$R_{ij} = log\left[p(H_i|x_j)\right] = log\left[p(x_j|H_i)P_i\right], \qquad (3)$$

where $p(x_j|H_i)$ is the probability density function of the local observation x_j conditioned on the hypothesis H_i, and P_i, $i = 1, ..., M$, are the prior probabilities of the hypotheses. We will propose (section II-C3) a method to estimate these prior probabilities from altimeter data. The detection mechanism eliminates the hypotheses with zero or negligible priors, and attempts to make a decision of choosing one among the remaining hypotheses. Detector j selects hypothesis H_{u_j}, where u_j is determined by the rule

$$u_j = \underset{1 \leq i \leq M}{\operatorname{argmax}}\{R_{ij}\}. \qquad (4)$$

The local decisions u_j, $j = 1, ..., N$ are transmitted to the fusion center for aggregation.

3) Global Fusion Rule: At the fusion center, the local decisions $\mathbf{u} = [u_1, ..., u_N]$ are fused to generate the final decision u such that the global probability of error is minimized. The fusion center computes the following test statistics $\forall i = 1, ..., M - 1$:

$$\begin{aligned} L_i &= log\left[\frac{p(H_i|\mathbf{u})}{p(H_M|\mathbf{u})}\right] \\ &= log\frac{P_i}{P_M} + \sum_{j \in S_1} log\left[\frac{(1 - \epsilon_j)(M - 1)}{\epsilon_j}\right] \\ &+ \sum_{j \in S_2} log\left[\frac{\epsilon_j}{(1 - \epsilon_j)(M - 1)}\right], \qquad (5) \end{aligned}$$

where P_i, $i = 1, ..., M$ are the prior probabilities of the hypotheses, with

$$\begin{aligned} S_1 &= \{j|u_j = i, \forall j = 1, ..., N\}, \\ S_2 &= \{j|u_j = M, \forall j = 1, ..., N\}, \end{aligned}$$

and ϵ_j is the probability of error of detector j defined as follows

$$\epsilon_j = \sum_{i=1}^{M} P_i \sum_{k=1, k \neq i}^{M} P(u_j = H_k|H_i). \qquad (6)$$

The fusion center makes the global decision by supporting H_u where u is computed according to the following fusion rule

$$u = \underset{1 \leq i \leq M}{\operatorname{argmax}}\{L_i\}. \qquad (7)$$

To implement the above decision fusion system, computation of the prior probabilities and the density functions of the observations conditioned on the hypotheses is required. In the subsequent sections we present new temporal evolution models for the local detector observations and outline methods to estimate the prior probabilities and the conditional probability

Table I: Hypoxia gradations based on SpO_2 and Functional Impairment ranges.

Hypotheses	Functional Impairment (%)	Probable Symptoms	$SpO_2(\%)$
H_1	0-1	No symptoms	92-100
H_2	1-10	Decreased night vision	85-92
H_3	10-50	Impaired recent memory and calculation	70-85
H_4	50-95	Altered judgment, impaired coordination	50-70
H_5	>95	Unconsciousness in minutes or seconds	<50

density functions. Specifically, in sections II-C1 and II-C2, we present first order time varying models describing the temporal evolution of blood oxygen saturation levels and functional impairment. In section II-C3, we discuss how such temporal models can be used to estimate prior probabilities. We also present the modeling of the conditional distributions of the observations.

C. Sensor Observation Models

We use blood oxygen saturation level (SpO_2) readings to develop a decision fusion scheme that can track temporal evolution of hypoxia. However, SpO_2 readings are known to stabilize at steady state values at any altitude where the subject resides. Typically, once steady state is attained, subsequent stay at a high altitude gradually induces hypoxia of increasing severity on the subject, while his/her SpO_2 readings remain approximately constant. This asymptotic behavior of SpO_2 readings means that sometimes SpO_2 level observations, by themselves, do not provide complete assessment of the likelihood of hypoxia. What is also needed is a measurement of the temporal effects of the (near constant) diminished SpO_2 levels in the subject. To this end, we propose to use the Percentage Functional Impairment ($\%FI$). Functional impairment is a health condition in which the normal function of a part of the body is less than its ideal full capacity [14]. The types of impairments that may be sustained range from mild physiological abnormalities (leading to a slight loss in function) to total impairment (often considered a full disability). Disability can refer to reduced functioning of physical and/or cognitive abilities. Here we propose a time varying model of SpO_2 variation with altitude and then offer a model that can predict a possible range of induced $\%FI$. We then show how these models could be used in estimating the prior probabilities used in the fusion scheme, and subsequently the degree of severity of hypoxia. We further compare the model predictions with real data sets. At every sampling instant k, based on the altitude value $A(k)$, the models compute blood oxygen saturation and functional impairment levels.

1) Blood oxygen saturation model: NASA earth atmospheric model [15], the alveolar equation ([16], page 92), and the modified Hill's equation [10] together predict the steady state SpO_2 values for any given altitude (see Appendix B for details). However, this approach does not take into consideration the transient phase of SpO_2 evolution during the ascent and descent phases of an altitude profile. We model the transient behavior of SpO_2 with change in altitude (ascent

or descent) using a first order non-homogeneous differential equation

$$\tau(A(t)) * \dot{s}(t) + s(t) = s_\infty. \qquad (8)$$

with initial condition $s(t')$, where t' is the most recent time of altitude change. In (8), $s(t)$ is the blood oxygen saturation level at time t, and s_∞ is the steady state blood oxygen saturation level for altitude $A(t)$ obtained from [10]. $\tau(A(t))$ is an altitude dependent time constant. The solution for $s(t)$ is

$$s(t) = s_\infty + (s(t') - s_\infty) * e^{-\left(\frac{(t-t')}{\tau(A(t))}\right)}. \qquad (9)$$

We implement the discretized version of (9), namely

$$s(k) = s_\infty + (s(k') - s_\infty) * e^{-\left(\frac{(k-k') \times T}{\tau(A(k))}\right)}. \qquad (10)$$

Here $t = k \times T$, T is the sampling time period, and k' is the most recent sampling instance of altitude change. The numerator in the exponent in (10) is the duration of stay of a subject at altitude $A(k)$.
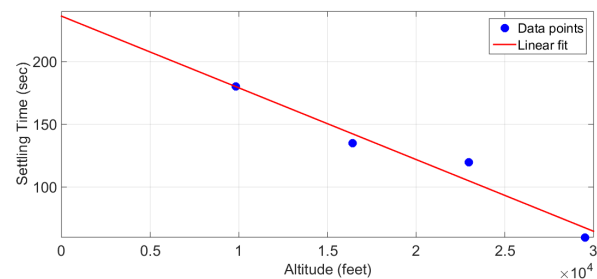

Figure 2: Linear least squares fit of SpO_2 settling times with altitude.

The SpO_2 settling times for the ascent phase are obtained by a linear least squares fit (see Fig. 2) of the data points in [17], (Fig. 24, p. 65), which provide settling time vs. altitude. During descent, the SpO_2 values increase and recovery occurs as the oxygen replenished blood is circulated throughout the body. Since an average adult human heart takes approximately 1 minute to circulate the entire blood volume in the human body ([18], page 207), the settling time for the descent phase is fixed at 60 sec. The time constant $\tau(A(k))$ for altitude $A(k)$ is obtained by dividing the settling time by 5. This is done in order to ensure that the transients reach 99% of the asymptotic value in a period of one time constant. In Fig. 3, we show the performance of the first order differential model (8) when applied to real data collected in the NAWCAD study [9]. The top trace shows the altitude profile. The bottom trace shows
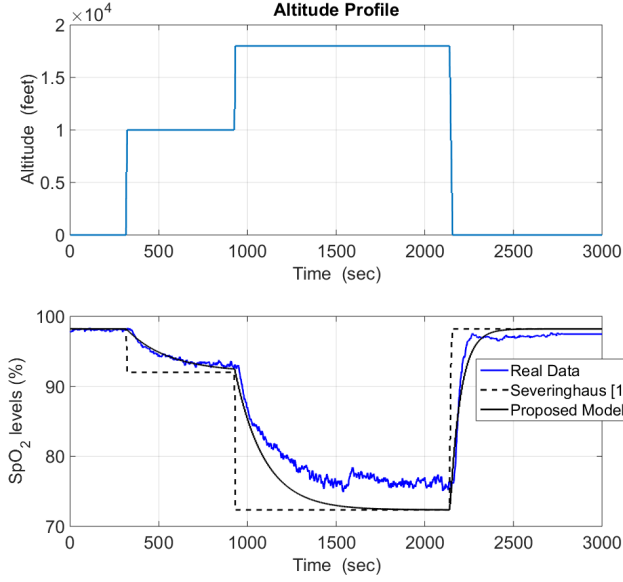
Figure 3: Comparison of proposed blood oxygen saturation temporal model with measured data and theoretical model of [10].

the SpO_2 readings from the three oximeters used for data collection after averaging. The steady state model in [10] and the proposed dynamic model for blood oxygen saturation in (8) are also shown. Our model achieved a root mean square (rms) error of 2.45% when fitted against the real data set compared to an rms error of 5.43% of the current existing theoretical model from [10].

2) Functional Impairment model: When exposed to high altitudes without adequate oxygen supply, humans gradually lose the ability to perform physical tasks efficiently and often also start suffering from impaired judgment. This loss of ability is termed as functional impairment, expressed in percentage, and denoted by $\%FI \in$[0, 100]. The average time period after which there is onset of such symptoms is referred to as the *Time of Useful Consciousness* (TUC) at that altitude (defined in [19], p. 97). Table 2 in ([20], p. 19) provides the various altitudes (in feet) and the corresponding ranges of TUC at those altitudes. We obtained the TUC range for other intermediate altitudes from this table through a cubic spline interpolation (other interpolation approaches are possible; the data for interpolation are available in [20]) . It was suggested in ([16], p. 97), that exposure to an altitude for a duration of TUC, leads to impaired judgment and loss of physical coordination. Under zero work load conditions, and absence of any external breathing assistance, exposure for length of time TUC is estimated to correspond to 50 $\%FI$ (see Table I). We model the temporal behavior of $\%FI$ using first order non-homogeneous differential equations. We begin by solving the following two separate systems:

$$\tau_1(A(t)) * \dot{z}_1(t) + z_1(t) = 0, \text{ and} \tag{11a}$$
$$\tau_2(A(t)) * \dot{z}_2(t) + z_2(t) = 100, \tag{11b}$$

with respective initial conditions denoted by IC_1 and IC_2, defined as

$$IC_1 = z_1(t'), \text{ and} \tag{12a}$$

$$IC_2 = \begin{cases} z_2(t'), & \text{if } \frac{dA(t)}{dt} \geq 0 \\ 0, & \text{otherwise.} \end{cases} \tag{12b}$$

Here, t' is the most recent time of altitude change, z_1 and z_2 are intermediate variables, $\tau_1(A(t)) = 5 \times r$, is a time constant with $r \in [1, 3]$ being the range of recovery time in minutes (recovery time assumes breathing air) taken to recover from hypoxic symptoms, $\tau_2(A(t))$, $(t \geq 0)$ are the TUC values corresponding to the altitude $A(t)$ scaled by $\frac{-1}{log(0.5)}$. The solutions for the systems in (11a) and (11b) are respectively

$$z_1(t) = (IC_1) \times e^{-(\frac{(t-t')}{\tau_1(A(t))})}, \tag{13a}$$

$$z_2(t) = 100 + ((IC_2) - 100) * e^{-(\frac{(t-t')}{\tau_2(A(t))})}. \tag{13b}$$

We implement the discretized versions of (13a) and (13b), which are provided below

$$z_1(k) = (IC_1) \times e^{-(\frac{(k-k') \times T}{\tau_1(A(k))})}, \tag{14a}$$

$$z_2(k) = 100 + ((IC_2) - 100) * e^{-(\frac{(k-k') \times T}{\tau_2(A(k))})}, \tag{14b}$$

where, T is the sampling period. Functional impairment is then computed as follows:

$$\%FI(k) \begin{cases} = 0, \text{ if } A(k) < 7000 ft, \\ \in 0 - 1\%, \text{ if } 7000 \leq A(k) < 15000 ft, \\ = \max(z_1(k), z_2(k)), \text{ if } A(k) \geq 15000 ft. \end{cases} \tag{15}$$

The assumptions in first and second cases of (15) are based on the discussion in ([21], page 1-21). $\%FI$ cannot be measured precisely. However, for any arbitrary altitude, for any duration of stay, using both the lower and upper limits of the TUC and recovery time (r), in (14a), (14b), and (15) we can get a range of the expected induced $\%FI$. Fig. 4 shows the $\%FI$ envelopes versus duration of stay for three different altitudes. For example, after spending 60 seconds at an altitude of 25000 feet while breathing air (no supplemental oxygen), the $\%FI$ induced ranges between 12% and 20%, (see Appendix C for an example). For any altitude profile, the computed range of $\%FI$ can thus provide estimates of the upper and lower envelopes of the possible hypoxia levels. The expected hypoxia level could vary between individuals but would generally fall within this envelope.

3) Modeling Priors and Conditional density functions: To investigate the performance of the fusion system, we have investigated two models of prior probabilities (P_i) and a method for calculating the conditional density functions ($P(x|H_i)$) of the observations. These are needed to compute the test statistics in (3) and (5).

Priors − Case I: We assume first that no altitude information is available. In this case, both the local detectors and the fusion center assume the hypotheses to have equal priors. In other words, for a set of M hypotheses, $P_i = 1/M$,
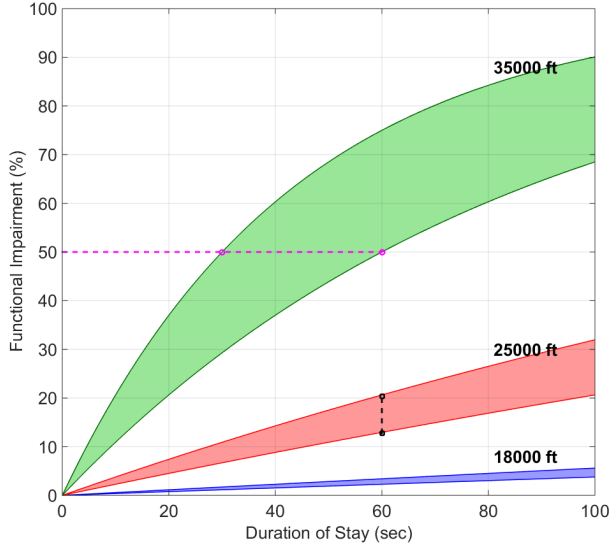
Figure 4: % Functional impairment versus duration of stay for three (3) different altitudes.

$$\forall i = 1, ..., M.$$

Priors – Case II: When the local detectors and the fusion center receive direct altimeter readings (see Fig. 1), the priors can be estimated more accurately. Using equations (14a), (14b), and (15), a range of $\%FI$ is computed for each altitude. We aim to learn where the calculated range falls with respect to the gradations defined in column 2 of Table I. To estimate the degree of overlap of the calculated range with the hypoxia gradations, we use a Gaussian distribution function of $\%FI$ with mean $m = \frac{r1+r2}{2}$ and standard deviation $\sigma = (m-r1)/3$, where the calculated $\%FI$ range is denoted by $[r1, r2]$. Integrating the Gaussian distribution function between the set bounds (column 2, Table I) provides the degree to which the calculated range supports each hypothesis. In other words, the degree of support for hypothesis H_i (denoted by mem_i), $i = 1, ..., M$ is given by

$$mem_i = \int_{low_i}^{up_i} G(x; m, \sigma). \tag{16}$$

Here low_i and up_i are the lower and upper limits defined in column 2 of Table I for hypothesis H_i, $G(x; m, \sigma)$ is the Gaussian distribution function parameterized by the mean m and standard deviation σ. The normalized support values provide estimates of the probabilities $p(H_i|A, k)$, $i = 1, ..., M$, where A is the altitude and k is the sampling instant, namely

$$p(H_i|A, k) = \frac{mem_i}{\sum_i mem_i}. \tag{17}$$

These estimates are used as priors $P_i(k) = p(H_i|A, k)$, $i = 1, ..., M$ in (3) and (5)[2]. For illustration, at an altitude of 25000 feet with a duration of stay of 60 seconds, the

range of $\%FI$ obtained is roughly $12 - 20\%$ (see Fig. 4). The associated Gaussian distribution function centered at the mean of the range (16%), with standard deviation of 1.33%, superimposed on the hypotheses set is shown in Fig. 5. The normalized support values toward the hypotheses set were computed as $H_1 : 0.0001$, $H_2 : 0.0667$, $H_3 : 0.9332$, $H_4 :\sim 0$, $H_5 :\sim 0$. In this case the detectors and the fusion center eliminate the last two hypotheses (H_4 and H_5) and use the decision rules defined in (3) and (5) with the hypothesis set now including only H_1, H_2, and H_3.

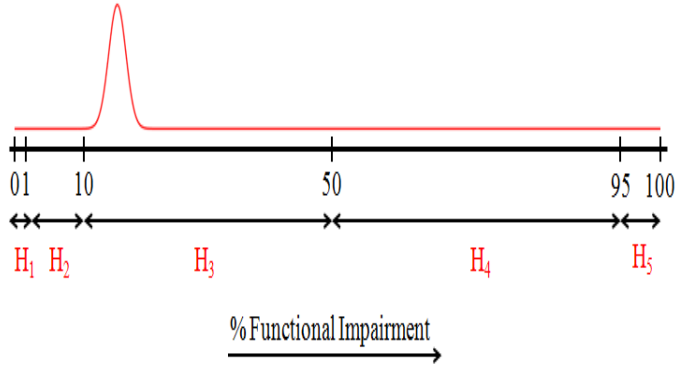There exist several studies that attempt to address the

Figure 5: Hypotheses gradations based on % Functional impairment with Gaussian density function centered on 16%

problem of on-line estimation of prior probabilities in a distributed detection framework (e.g., [22], [23]). Variants of these algorithms may also be used in the context of the current study.

Conditional density functions: To implement the decision rules in (4), the local detectors need to compute the conditional probabilities $p(x_j|H_i)$, $\forall i = 1, ..., M; j = 1, ..., N$. In this case, the local observations, x, are SpO_2 readings. They are represented as real numbers between 0 and 1 and assumed to be Beta distributed under each hypotheses for each local detector. In other words,

$$p(x_j|H_i) \sim \mathcal{B}(\alpha_{ij}, \beta_{ij}), \forall i = 1, ..., M; j = 1, ..., N.$$

We use the data sets recorded in the NAWCAD study [9] (see section II-A) and employ a maximum likelihood technique to estimate the Beta distribution parameters $(\alpha_{ij}, \beta_{ij})$ under each hypothesis. One of the primary reasons for choosing the Beta distribution is its versatility in modeling both skewed and symmetrical data sets that are bound within a finite range (e.g., [24]). A parametric model for the conditional densities (as opposed to a non-parametric model developed using kernel based methods) would also allow the hypoxia detection scheme to be executed in real time.

III. RESULTS

For performance analysis, we tested the M-ary decision fusion system shown in Fig. 1 using both synthetic and real

data sets. Synthetic data sets enabled model validation and analysis of global detection performance. The applicability and robustness of the scheme were then verified from testing with real data.

For any recorded altitude profile, upper and lower envelopes of $\%FI$ were computed using equations (14a), (14b), and (15). Depending on where the upper and lower bounds of the $\%FI$ range fall with respect to the gradations defined in column 2 of Table I, a band of possible true hypotheses were assigned to each observation. If a local or global decision fell outside this band, it was considered an error; else the decision was considered correct. Each detector was tested against multiple data sets and the percentage of the detector's wrong decisions was computed for each data set. The error probabilities ϵ_j, $j = 1, ..., N$ in (5) were calculated as the percentage of wrong decisions for each detector averaged over the entire data set.

A. Testing with synthetic data

A random set of 200 different altitude profiles was simulated. Each individual profile peaked randomly at different altitudes between 5000 ft (1524 m) and 25000 ft (7620 m) and had varying duration of stay at the peaks. For each altitude profile, a corresponding blood oxygen saturation signal (SpO_2) was generated with the help of the model defined in (9). Using the colored noise models derived for each oximeter in [11], the local observations were simulated as the SpO_2 signal embedded in colored noise. Fig. 6 shows a sample simulated altitude profile (top trace) and the simulated SpO_2 signal (second trace). The simulated noisy local sensor signals and associated Kalman filtered signals are shown in the bottom three traces.
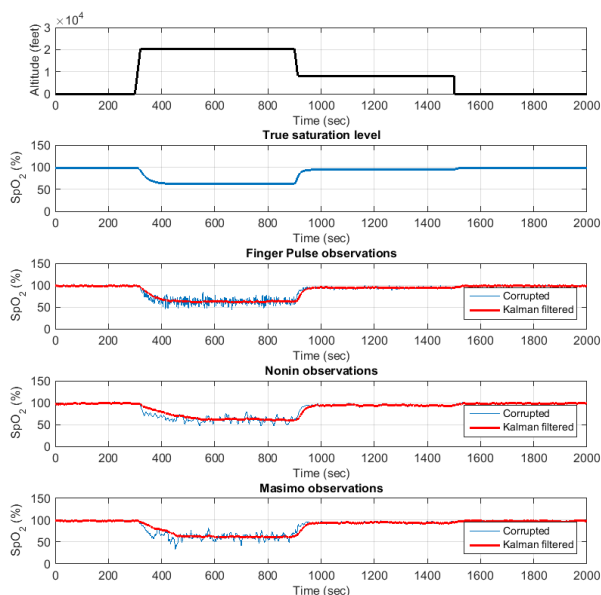

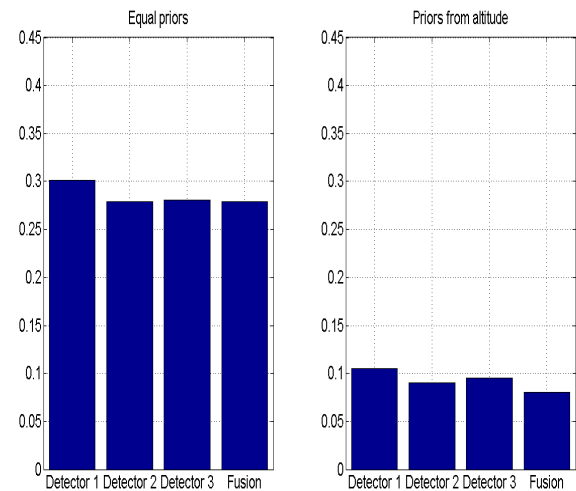Figure 6: Synthetic altitude profile and simulated oximeter observations.

Figure 7: Averaged local and global error rates with synthetic data.

We show the average performance after decision fusion in Fig. 7. The left-hand figure shows the error rates achieved by the three local detectors and the fusion center when the prior probabilities were assumed to be equal. The global error rate was computed to be 0.279. The right-hand figure shows the local and global error rates achieved when priors were computed using the information from the altitude and the duration of stay at the altitude. Using functional impairment to estimate the priors improves the detection performance significantly. The global error rate was computed to be 0.08 (a 71% improvement over the case when equi-probable priors were assumed). Figures. 8, 9, 10 compare the empirical and model cumulative distribution functions (cdf) of the observed data. The top trace in each figure shows the Beta distribution of blood oxygen saturation levels under each hypotheses for a particular oximeter. Maximum likelihood parameter estimates of the Beta distribution parameters were obtained from the simulated SpO_2 readings. The bottom traces show the empirical and model cumulative distribution functions (cdf) for the three sensor observations. It appears that for practical purposes, the Beta distribution models can be used to approximate the distribution of the observed data.

B. Testing with measured data

The M-ary decision fusion system shown in Fig. 1 was tested against 34 data sets captured from 17 different individual subjects (2 data sets recorded from each subject against a fixed altitude profile), collected in the study at NAWCAD [9]. This excludes the trials that experienced sensor data drops. Fig. 11 shows a sample data set of three oximeter readings with the simulated altitude profile from one of the subjects. The Kalman filtered signals were used for local decision making.

Fig. 12 shows the averaged error rates (averaged over the 34 individually analyzed runs) at the local detectors and the fusion center. The left-hand figure shows the local and global error rates when equal prior probabilities were assumed. The
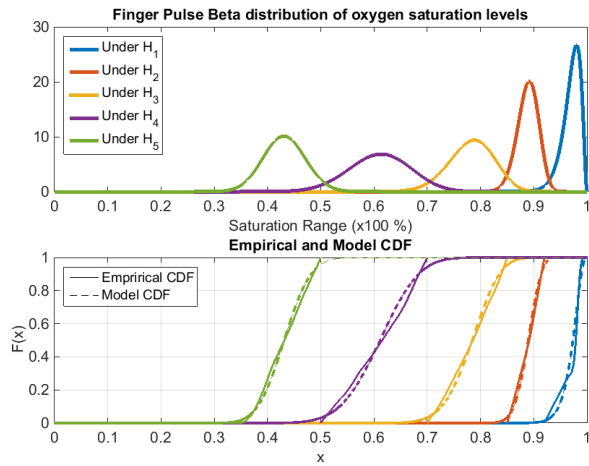
Figure 8: Model and empirical distributions of SpO_2 values from synthetic data set under each hypothesis for detector 1.
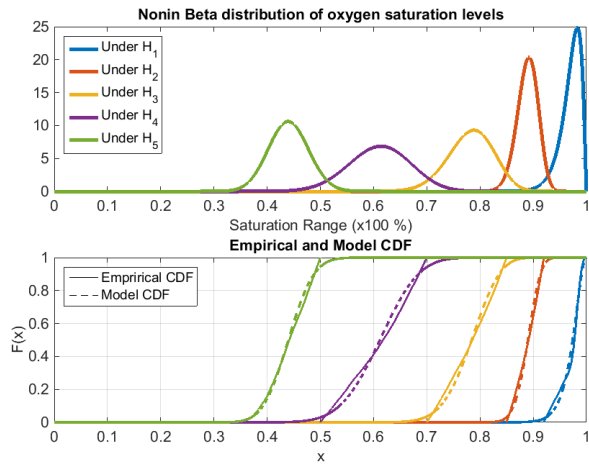

Figure 9: Model and empirical distributions of SpO_2 values from synthetic data set under each hypothesis for detector 2.
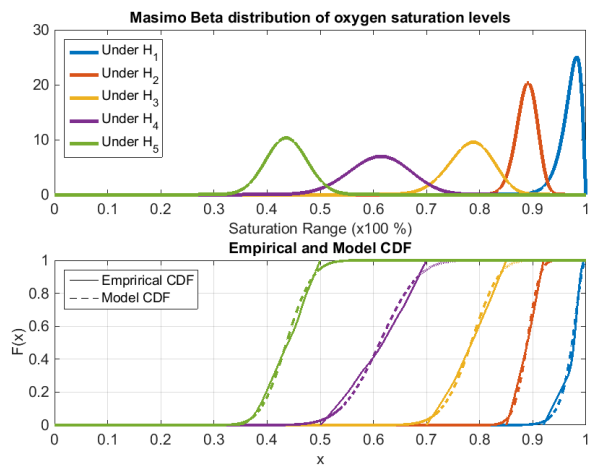

Figure 10: Model and empirical distributions of SpO_2 values from synthetic data set under each hypothesis for detector 3.
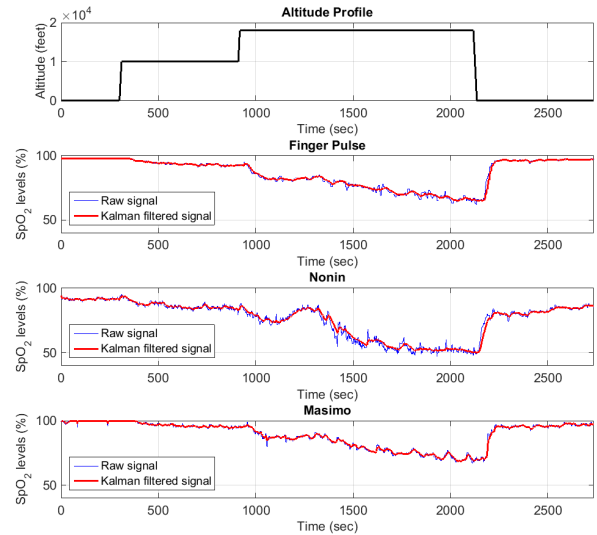

Figure 11: Original and Kalman filtered pulse oximeter signals from a single subject.
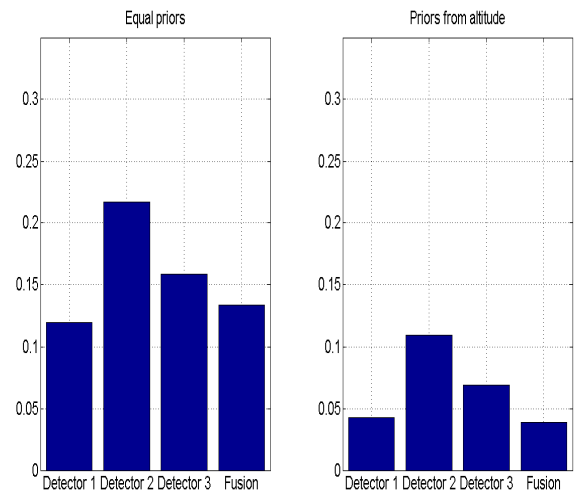

Figure 12: Averaged local and global error rates with measured data. Detector 1 is Finger pulse, Detector 2 is Nonin and Detector 3 is Masimo oximeters.

hand figure shows the system performance when the prior probabilities were estimated from functional impairment. The global error rate reduced to 0.039 (approximately a 70% improvement). Figures 13, 14, 15 compare the empirical cdf of the data set with the Beta distribution models. The top traces show the Beta distributions of the observations under each hypothesis for each oximeter. The bottom traces show the empirical and model cdf. The model approximately follows the trends in the actual data sets[3].

Fig. 16 shows the fusion result for a single subject. The top trace has the altitude profile. The second, third and fourth

fusion center attained a global error rate of 0.134. The right-

[3] For the altitude profile used in the real data set, no oximeters except Nonin recorded SpO_2 readings in the H_5 category.

This article has been accepted for publication in a future issue of this journal, but has not been fully edited. Content may change prior to final publication. Citation information: DOI 10.1109/JBHI.2016.2528887, IEEE Journal of Biomedical and Health Informatics
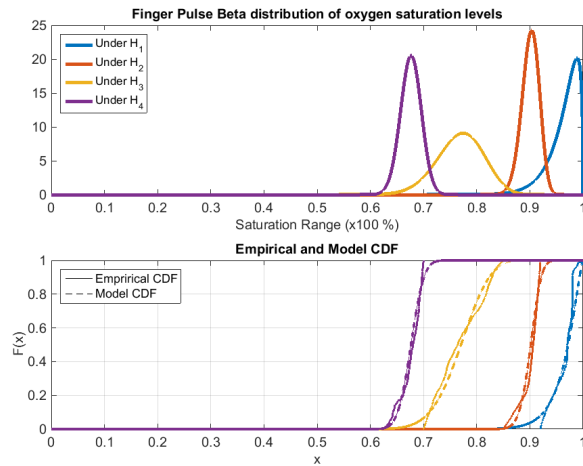
9

Figure 13: Model and empirical distributions of SpO_2 values from measured data set under each hypothesis for Finger Pulse.
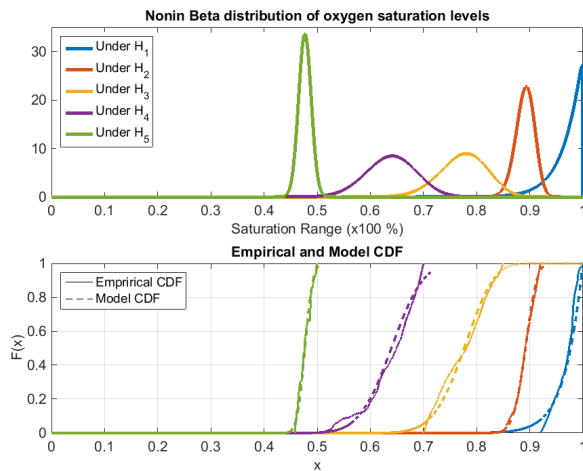

Figure 14: Model and empirical distributions of SpO_2 values from measured data set under each hypothesis for Nonin.
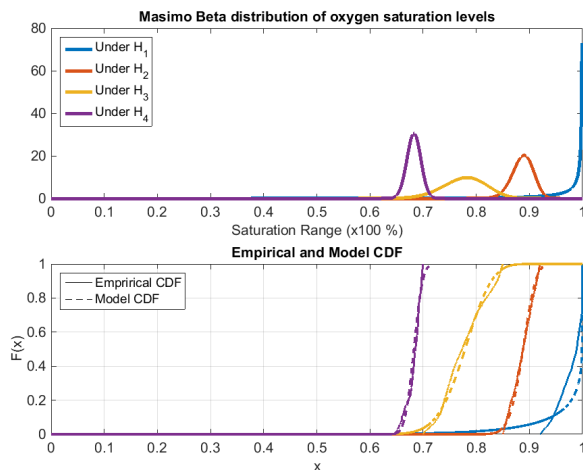

Figure 15: Model and empirical distributions of SpO_2 values from measured data set under each hypothesis for Masimo.
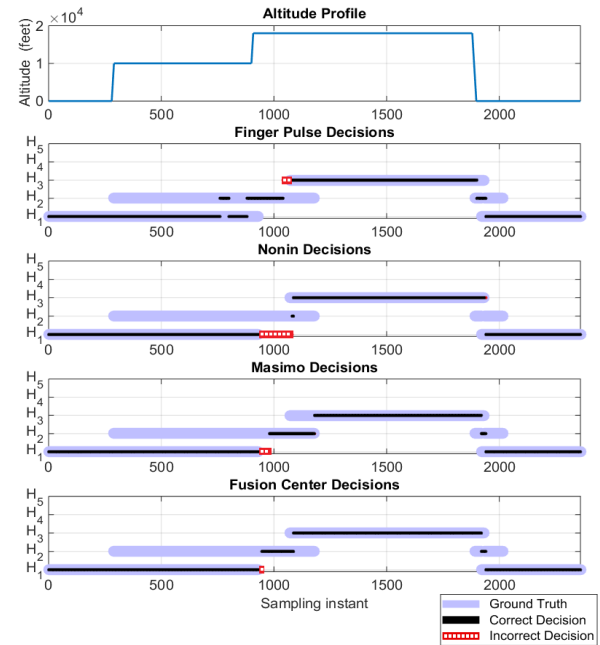

Figure 16: Sample fusion result for a single subject.

traces show the local detector decisions. The bottom trace shows the fusion center decisions. The red regions mark the instants when local detectors or the fusion center decided incorrectly. The black regions mark the correct decisions. The ground truth is shown with the light blue band (note that, during some time instants, instead of a single hypothesis, the blue bands define a range of true hypotheses, choosing anyone among which would be considered correct).

IV. DISCUSSION AND FUTURE WORK

We developed a real time hypoxia detection architecture, which takes signals from pulse oximeters attached to a subject and from altimeters, and estimates a category of severity of hypoxia. The use of Kalman filtering on the raw pulse oximeter outputs and the implementation of decision fusion aided in creating a system that is more robust and reliable than a system based on a single sensor and its observed signal. The input signals to the system (blood oxygen saturation levels and altitude readings) are available from inexpensive sensors. The parallel fusion architecture makes the system modular, i.e., malfunctioning sensors can be removed or ignored, and new sensors can be added easily without affecting the local and global detection rules.

The oximeter observations were modeled using the uni-modal Beta distribution. However, the mode of the distributions under each hypothesis might possibly shift as a function of the altitude and duration of stay. For example, the most probable SpO_2 value under H_1 at an altitude of 15000 feet might be different than the most probable value under the same hypothesis at an altitude of 1000 feet. Furthermore, staying at an altitude of 15000 feet for some period of time might also shift the mode (it might gradually decrease). Modeling this shift of skewness of the distributions, as altitude and duration

at the altitude vary, may further improve hypoxia category estimation. We suggested a method for estimating the prior probabilities of the hypoxia categories based on duration of stay of a subject at an altitude. This method uses the concept of functional impairment (FI) and significantly improves the overall detection performance as compared to simply assuming equal priors.

The current study presents a generic multi-sensor model for detecting hypoxia in real time. It does not address individual physiologic tolerances. The system estimates functional impairment (FI) based on altitude and ranges of average duration of stay at that altitude. We used broad Time of Useful Consciousness (TUC) ranges to facilitate the estimation.

If individual tolerances and other physiological traits are available, these can be used to estimate the FI better for specific individuals. Incorporating such estimates would make the hypoxia detection system better-suited to address individual subject variability.

We have used data from subjects who were not exposed to strenuous workloads. If the subject is exercising, or otherwise under a stressful workload, the bounds on TUC may change. Obtaining TUC bounds under various workload conditions is likely to improve the calculation of priors. Furthermore, it is known that there are effects like acceleration atelectasis which affect the blood oxygen saturation levels in the human body ([25], [26]). Investigating the effects of acceleration (such as the effects of high G maneuvers) on the blood oxygen saturation levels, and the functional impairment they induce, would further improve the underlying model. Incorporation of the effects of acceleration is required for health monitoring of air crews (such as high performance aircraft pilots).

A. Limitations

The hypoxia prediction system presented in this study is based on certain assumptions which may limit its applicability.

1) The sensor configuration uses multiple oximeters attached to the finger and forehead. This configuration may be too cumbersome for continuous use by active individuals. It may also be affected by motion artifacts. Recently new devices such as ring oximeters ([27], [28]) were developed to address this challenge.

2) Scattering of light from commonly-illuminated volumes and other interferences may reduce oximeter measurement quality and introduce correlation between local-detector decisions. To reduce internal interference between signals captured from multiple reflectance-type oximeters, the oximeters in our experiments were placed on the subject's forehead so as to maximize the physical separation between them. However, such precautions might still not completely suppress interference and correlation. If appreciable correlation between local decisions is present, a version of the decision rule we introduced in section II-B3 can be used that takes into account correlated decisions [29].

3) The present study does not take into account the effects of altitude acclimatization by the subjects. In its current form the study is therefore suitable for hypoxia

prediction under short exposures of approximately 20-30 minutes. Furthermore, the TUC ranges provided in ([20], p. 19) do not give an upper limit for the TUC at 15,000 ft. The assumptions we made in (15) are conservative: we assumed for 15,000 ft the same limits as those provided in [20] for 18,000 ft. Between 7000 ft and 15,000 ft we use a fixed range for functional impairment based on the discussion in reference ([21], page 1-21, paragraph 2). More accurate estimates of FI may be developed in time for these lower heights.

4) Our test data were collected under normobaric conditions. These data are likely to be different from data collected in an altitude chamber, where the variation of atmospheric pressure is taken into account as well. Recent studies ([30], [31]) have shown that hypobaria can have effects on the onset and severity of hypoxia. The models presented here do not include such effects. If data from hypobaric conditions are made available, the methodology provided in this study can be used to re-estimate the key parameters and recalculate the hypoxia estimates.

V. CONCLUSION

We developed a real time hypoxia detection architecture that can predict the degree of induced hypoxia in humans as a function of the duration of exposure to different altitude profiles. We tested the architecture on synthetic data as well as actual measurements. We presented new temporal evolution models using first order non-homogeneous differential equations for blood oxygen saturation levels (SpO_2) and percentage functional impairment ($\%FI$). Our proposed models used clinically verified Time of Useful Consciousness (TUC) ranges and improved real time hypoxia monitoring of normal and healthy individuals. The likelihood of the severity of induced hypoxia was estimated by using altitude and duration of stay of a subject at that altitude. A parallel detection framework made the system modular and robust to single-sensor failures. The models were compared against synthetic and real data sets for performance analysis. When tested against real data sets, the framework attained an overall error rate of 0.039, namely the severity of hypoxia was estimated correctly in more than 96% of cases.

ACKNOWLEDGMENT

APPENDIX A
KALMAN FILTER MODEL

We consider the blood oxygen saturation level (in %) as the scalar state x and define its dynamics as the first order system

$$x(k) = Fx(k-1) + w(k). \qquad (18)$$

$x(k)$ is the blood oxygen saturation level at time instant k. The system matrix F is considered to be constant, equal to 1.

This article has been accepted for publication in a future issue of this journal, but has not been fully edited. Content may change prior to final publication. Citation information: DOI 10.1109/JBHI.2016.2528887, IEEE Journal of Biomedical and Health Informatics

11

$w(k)$ is the zero mean Gaussian process noise with variance Q. The state observation model is

$$z^i(k) = H(k)x(k) + v^i(k), \qquad (19)$$

where $z^i(k)$ and $v^i(k)$ are, respectively, the observation (noisy blood oxygen saturation level) and the measurement noise of the ith oximeter, $H(k)$ is the observation matrix at time instant k ($H(k) = 1$ for our model). Oximeter measurements were found to be temporally correlated with data dependent variance [11]. The measurement noise of each oximeter are modeled as the output of a second order Autoregressive (AR) process driven by zero mean white Gaussian noise. The AR(2) model for a colored observation signal $v(k)$ (measurement noise from an oximeter) is

$$v(k) = a_1 v(k-1) + a_2 v(k-2) + e(k), \qquad (20)$$

where a_j for $j = 1, 2$ are the AR parameters and $e(k) \sim \mathcal{N}(0, \sigma_e^2(k))$ is zero mean Gaussian noise input to the AR system. We follow the standard state augmentation approach ([32], section 7.2) to incorporate colored measurement noise in the Kalman filter formulation. The approach augments the the actual state vector $x(k)$ in (18) with the colored noise samples $v^i(k)$ which are the output of a linear system as defined in (20). The original system in (18) is augmented as shown in (21), $a_j^i, i = 1, 2, 3$ and $j = 1, 2$ are the AR parameters for the ith oximeter. $e^i(k)$ is the input at time instant k for the AR model of the ith oximeter measurement noise (see (20)).

$$\begin{bmatrix} x(k) \\ v^i(k) \\ v^i(k-1) \end{bmatrix} = \begin{bmatrix} F & 0 & 0 \\ 0 & a_1^i & a_2^i \\ 0 & 1 & 0 \end{bmatrix} \begin{bmatrix} x(k-1) \\ v^i(k-1) \\ v^i(k-2) \end{bmatrix} + \begin{bmatrix} w(k) \\ e^i(k) \\ 0 \end{bmatrix} \quad (21)$$

The corresponding augmented measurement equation for the ith oximeter becomes

$$z^i(k) = \begin{bmatrix} 1 & 1 & 0 \end{bmatrix} \begin{bmatrix} x(k) \\ v^i(k) \\ v^i(k-1) \end{bmatrix} \qquad (22)$$

The formulation in (21) and (22) form the standard Kalman filter model used to obtain an estimate of the blood oxygen saturation level.

APPENDIX B
STEADY STATE BLOOD OXYGEN SATURATION MODEL

The current theoretical model [10] that predicts blood oxygen saturation levels as a function of altitude computes only the steady state saturation values. This model is derived in three steps.

Step 1: NASA earth atmospheric model [15], computes the barometric pressure from altitude A.

For Troposphere ($A < 36152 ft$),

$$T = 59 - 0.00356 * A,$$

$$\text{P\textsubscript{B}} = 2116 * \left(\frac{T + 459.7}{518.6}\right)^{5.256}.$$

For Lower Stratosphere ($36152 ft < A < 82345 ft$),

$$T = -70,$$

$$\text{P\textsubscript{B}} = 473.1 * e^{(1.73 - 0.000048 * A)}.$$

For Upper Stratosphere ($A > 82345 ft$),

$$T = -205.5 + 0.00164 * A,$$

$$\text{P\textsubscript{B}} = 51.97 * \left(\frac{T + 459.7}{389.98}\right)^{-11.388}.$$

Here, 'A' is the altitude in feet (ft), 'T' is the temperature in degree Fahrenheit ($^o F$), and 'P\textsubscript{B}' is the barometric pressure in lbs/ft^2.

Step 2: The alveolar gas equation ([16], page 92) uses the barometric pressure as computed in Step 1 to generate the mean alveolar oxygen pressure as follows

$$\text{PA}_{O_2} = (\text{P\textsubscript{B}} - \text{PH}_2\text{O}) * \text{FI}_{O_2} - \text{PA}_{CO_2} * \left(\text{FI}_{O_2} + \frac{1 - \text{FI}_{O_2}}{\text{RQ}}\right),$$

where, 'PA$_{O_2}$' is the mean alveolar oxygen pressure, 'P\textsubscript{B}' is the ambient barometric pressure, 'PH$_2$O' is the water vapor pressure at body temperature, 'PA$_{CO_2}$' is the mean alveolar carbon dioxide pressure, all in lbs/ft^2, 'FI$_{O_2}$' is the fraction of inspired oxygen, and 'RQ' is the respiratory quotient.

Step 3: In the final step, the modified Hill's equation [10] produces estimates of blood oxygen saturation as follows

$$S = (((\text{PA}_{O_2}{}^3 + 150 * \text{PA}_{O_2})^{-1} * 23400) + 1)^{-1},$$

where, 'PA$_{O_2}$' is the mean alveolar oxygen pressure and 'S' is the blood oxygen saturation.

APPENDIX C
CALCULATION OF FUNCTIONAL IMPAIRMENT ENVELOPES

Example: Let us assume an individual is exposed to an altitude profile similar to the one shown in the top trace of Fig. 17. The duration of stay at every altitude is shown along the x-axis of the bottom trace. Using both the lower and upper limits of TUC and recovery time (r), (14a) and (14b) generate ranges of the intermediate variables z_1 and z_2. The striped band in the bottom trace of Fig. 17 is the solution obtained from (14a), whereas the plain band is generated by (14b). The functional impairment $\%FI$ is the maximum of these two bands (see third case in (15)) and is shown by black envelope.

The $\%FI$ of the subject at the beginning of the altitude profile is assumed to be 0%. The altitude changes at time instants $t = 400$ and $t = 800$. This results in change of initial conditions according to (12a) and (12b). Substituting the new initial conditions in (14a) and (14b) at time instants $t = 400$ and $t = 800$ causes the discontinuities in the intermediate variables z_1 and z_2 (striped and plain bands respectively).
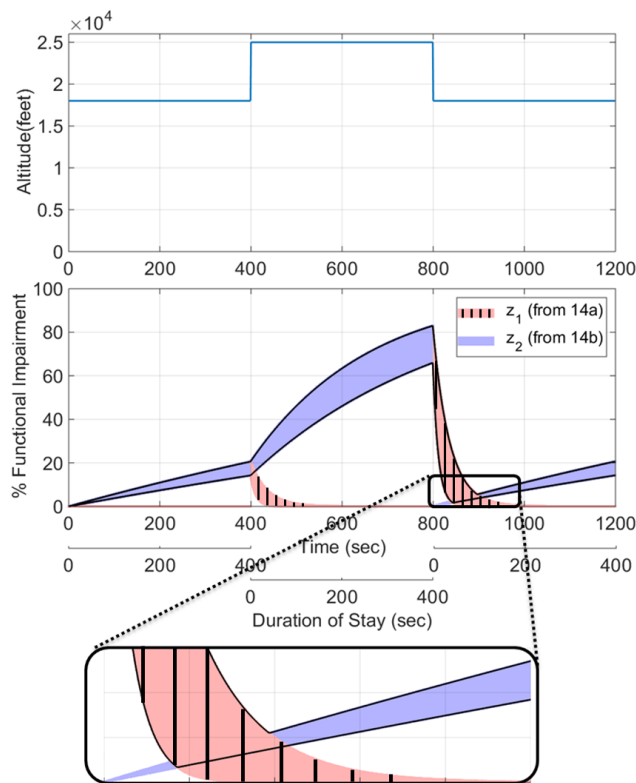
Figure 17: % Functional impairment versus time for sample ascent and descent altitude profile.

REFERENCES

[1] A. C. Guyton, "Textbook of Medical Physiology," *The American Journal of the Medical Sciences*, vol. 242, no. 2, p. 136, 1961.

[2] S. R. Crouch and J. D. Ingle, *Spectrochemical Analysis*. Prentice Hall, 1988.

[3] J. E. Sinex, "Pulse Oximetry: Principles and Limitations," *The American Journal of Emergency Medicine*, vol. 17, no. 1, pp. 59–66, 1999.

[4] "Aviation Hypoxia Monitor," US Patent 5,372,134, 1994. [Online]. Available: http://patft.uspto.gov/netacgi/nph-Parser?Sect2=PTO1& Sect2=HITOFF&p=1&u=/netahtml/PTO/search-bool.html&r=1&f=G& l=50&d=PALL&RefSrch=yes&Query=PN/5372134

[5] M. Kelly and D. Pettit, "Oxygen-Partial-Pressure Sensor for Aircraft Oxygen Mask," *NASA Tech Briefs*, 2003.

[6] R. Gurjar, M. Seetamraju, D. E. Wolf, and J. Hastings, "High Reliability, Miniature Personal Hypoxia Monitoring System," in *SPIE Defense, Security, and Sensing*. International Society for Optics and Photonics, pp. 76 740H–76 740H, 2010.

[7] A. Jubran, "Pulse Oximetry," *Crit Care*, vol. 3, no. 2, pp. R11–R17, 1999.

[8] D. Clayton, R. Webb, A. Ralston, D. Duthie, and W. Runciman, "Pulse Oximeter Probes: A Comparison between Finger, Nose, Ear and Forehead Probes under Conditions of Poor Perfusion*," *Anaesthesia*, vol. 46, no. 4, pp. 260–265, 1991.

[9] B. Shender, C. Mattingly, M. Warren, S. Coleman, G. Askew, and A. Tucker, "Relating the Time Complex Cognitive Performance Degrades to Physiologic Response During Moderate and Severe Normobaric Hypoxia," *Aviation, Space, and Environmental Medicine*, vol. 84, no. 4, p. 340, 2013.

[10] J. W. Severinghaus, "Simple, Accurate Equations for Human Blood o2 Dissociation Computations," *Journal of Applied Physiology*, vol. 46, no. 3, pp. 599–602, 1979.

[11] S. Acharya, A. Rajasekar, B. Shender, L. Hrebien, and M. Kam, "Pulse oximeter signal modeling and fusion for hypoxia monitoring," in *17th International Conference on Information Fusion (FUSION)*, pp. 1–8, July, 2014.

[12] J. F. Parker Jr and V. R. West, "Bioastronautics Data Book: Nasa sp-3006." *NASA Special Publication*, vol. 3006, 1973.

[13] W. Baek, "Optimal m-ary Data Fusion with Distributed Sensors," *IEEE Transactions on Aerospace and Electronic Systems*, vol. 31, no. 3, pp. 1150–1152, Jul 1995.

[14] (2003) Miller-keane Encyclopedia and Dictionary of Medicine, Nursing, and Allied Health. [Online]. Available: http://medical-dictionary. thefreedictionary.com/impairment

[15] Earth Atmosphere Model. [Online]. Available: www.grc.nasa.gov/www/ k-12/airplane/atmosmet.html

[16] J. R. Davis, R. Johnson, and J. Stepanek, *Fundamentals of Aerospace Medicine*. Lippincott Williams & Wilkins, 2008.

[17] H. W. Randel and H. G. Armstrong, *Aerospace Medicine*. Williams & Wilkins, 1971.

[18] A. Guyton, *Textbook of Medical Physiology*, 4th ed. Saunders (W.B) Co Ltd, February 1971.

[19] R. DeHart, Ed., *Fundamentals of Aerospace Medicine*. Lea & Febiger, 1985.

[20] D. R. Jenkins, *Dressing for Altitude: U.S. Aviation Pressure Suits, Wiley Post to Space Shuttle (NASA Sp)*, ser. The NASA Aeronautic Series. National Aeronautics and Space Administration (NASA), August 2012.

[21] R. Michael, C. James, G. Annette *et al.*, "US Naval Flight Surgeon's Manual," 1991.

[22] A. Naim and M. Kam, "On-line Estimation of Probabilities for Distributed Bayesian Detection," *Automatica*, vol. 30, no. 4, pp. 633–642, 1994.

[23] G. Mirjalily, Z.-Q. Luo, T. N. Davidson, and E. Bosse, "Blind Adaptive Decision Fusion for Distributed Detection," *IEEE Transactions on Aerospace and Electronic Systems*, vol. 39, no. 1, pp. 34–52, 2003.

[24] R. Krzysztofowicz and D. Long, "Fusion of Detection Probabilities and Comparison of Multisensor Systems," *IEEE Transactions on Systems, Man and Cybernetics*, vol. 20, no. 3, pp. 665–677, 1990.

[25] W. Tacker Jr, U. Balldin, R. Burton, D. Glaister, K. Gillingham, and J. Mercer, "Induction and Prevention of Acceleration Atelectasis." *Aviation, Space, and Environmental Medicine*, vol. 58, no. 1, pp. 69–75, 1987.

[26] M. Haswell, W. Tacker Jr, U. Balldin, and R. Burton, "Influence of Inspired Oxygen Concentration on Acceleration Atelectasis." *Aviation, Space, and Environmental Medicine*, vol. 57, no. 5, pp. 432–437, 1986.

[27] C.-Y. Huang, M.-C. Chan, C.-Y. Chen, and B.-S. Lin, "Novel Wearable and Wireless Ring-Type Pulse Oximeter with Multi-Detectors," *Sensors*, vol. 14, no. 9, pp. 17 586–17 599, 2014.

[28] A. Kishimoto, O. Tochikubo, K. Ohshige, and A. Yanaga, "Ring-shaped Pulse Oximeter and its Application: Measurement of Spo2 and Blood Pressure During Sleep and During Flight," *Clinical and Experimental Hypertension*, vol. 27, no. 2-3, pp. 279–288, 2005.

[29] M. Kam, Q. Zhu, and W. S. Gray, "Optimal Data Fusion of Correlated Local Decisions in Multiple Sensor Detection Systems," *IEEE Transactions on Aerospace and Electronic Systems,*, vol. 28, no. 3, pp. 916–920, 1992.

[30] B. A. Beidleman, C. S. Fulco, J. E. Staab, S. P. Andrew, and S. R. Muza, "Cycling Performance Decrement is Greater in Hypobaric versus Normobaric Hypoxia," *Extreme Physiol Med*, vol. 3, no. 8, pp. 10–1186, 2014.

[31] D. M. DiPasquale, G. E. Strangman, N. S. Harris, and S. R. Muza, "Hypoxia, Hypobaria, and Exercise Duration Affect Acute Mountain Sickness," *Aerospace Medicine and Human Performance*, vol. 86, no. 7, pp. 614–619, 2015.

[32] D. Simon, *Optimal State Estimation: Kalman, H Infinity, and Nonlinear Approaches*. John Wiley & Sons, 2006.